Original Research

Radiomics in the CT diagnosis of ovarian cystic malignancies - a pilot study

Lucian Mărginean[1,2], Paul-Andrei Ștefan[2,3,4,5], Rareș Cristian Filep[1,2], Csaba Csutak[5,6], Andrei Lebovici[5,6], Diana Gherman[5,6], Roxana-Adelina Lupean[7,8], Bogdan Andrei Suciu[9,10]

MEDICAL IMAGING

1) Radiology and Medical Imaging, Clinical Sciences Department, "George Emil Palade" University of Medicine, Pharmacy, Science, and Technology, Târgu Mureș, Romania

2) Interventional Radiology Department, Târgu Mureș County Emergency Clinical Hospital, Târgu Mureș, Romania

3) Department of Biomedical Imaging and Image-Guided Therapy, General Hospital of Vienna (AKH), Medical University of Vienna, Austria

4) Department of Anatomy and Embriology, Morphological Sciences, Iuliu Hatieganu University of Medicine and Pharmacy, Cluj-Napoca, Romania

5) Department of Radiology and Imaging, Cluj County Emergency Clinical Hospital, Cluj-Napoca, Romania

6) Department of Radiology and Imaging, Surgical Specialties, Iuliu Hatieganu University of Medicine and Pharmacy, Cluj-Napoca, Romania

7) Department of Histology, Morphological Sciences, Iuliu Hatieganu University of Medicine and Pharmacy, Cluj-Napoca, Romania

8) "Dominic Stanca" Obstetrics and Gynecology Clinic, Cluj County Emergency Clinical Hospital, Cluj-Napoca, Romania

9) First Surgical Clinic, Târgu Mureș County Emergency Clinical Hospital, Târgu Mureș, Romania

10) Department of Anatomy, Morphological Sciences, "George Emil Palade" University of Medicine, Pharmacy, Science, and Technology, Târgu Mureș, Romania

Abstract

Background and aims. The conventional computed tomography (CT) appearance of ovarian cystic masses is often insufficient to adequately differentiate between benign and malignant entities. This study aims to investigate whether texture analysis of the fluid component can augment the CT diagnosis of ovarian cystic tumors.

Methods. Eighty-four patients with adnexal cystic lesions who underwent CT examinations were retrospectively included. All patients had a final diagnosis that was established by histological analysis in forty four cases. The texture features of the lesions content were extracted using dedicated software and further used for comparing benign and malignant lesions, primary tumors and metastases, malignant and borderline lesions, and benign and borderline lesions. Texture features' discriminatory ability was evaluated through univariate and receiver operating characteristics analysis and also by the use of the k-nearest-neighbor classifier.

Results. The univariate analysis showed statistically significant results when comparing benign and malignant lesions (the Difference Variance parameter, p=0.0074) and malignant and borderline tumors (the Correlation parameter, p=0.488). The highest accuracy (83.33%) was achieved by the classifier when discriminating primary tumors from ovarian metastases.

Conclusion. Texture parameters were able to successfully discriminate between different types of ovarian cystic lesions based on their content, but it is not entirely clear whether these differences are a result of the physical properties of the fluids or their appartenance to a particular histopathological group. If further validated, radiomics can offer a rapid and non-invasive alternative in the diagnosis of ovarian cystic tumors.

Keywords: computed tomography, ovary, radiomics, texture analysis

DOI: 10.15386/mpr-2594

Manuscript received: 05.12.2022
Received in revised form: 07.02.2023
Accepted: 06.03.2023

Address for correspondence:
Paul Andrei Ștefan
stefan_paul@ymail.com

Background and aims

Ovarian cysts represent a common gynecological disorder, being the result of physiological or pathological processes [1]. Ultrasonography represents the first-line imaging method for investigating ovarian lesions [2], while computed tomography (CT) is usually reserved for evaluation in the pretreatment planning of a suspected adnexal malignancy [3].

One of the most important goals of imaging in the characterization of ovarian masses is the distinction between malignant and benign lesions [4], considering its major impact on subsequent medical and surgical management [5]. Most of the time, when analyzing CT images of an ovarian cyst, physicians do not pay particular attention to the liquid content, mainly focusing on finding attributes advocating for malignancy (multilocularity, irregular and thickened cystic septs, internal vegetations etc.) [4]. However, these features are not always pathognomonic,

especially because many benign ovarian tumors of mixed type (with solid and liquid components) can mimic a malignant lesion [5,6].

On the other hand, the pathological examination of ovarian cysts reveals specific characteristics regarding their fluid composition, which can be typical for certain diseases [7]. These characteristics are related to the physical properties (clarity, color, homogeneity), as well as to the cellularity and chemical composition of the contained fluids [8,9]. Although the pathological features are difficult to be quantified visually on CT images, they may have a significant influence on the intensity and distribution of the pixels within an image [10].

The differences between the pixel intensities define the texture of an image, which can be more or less perceptible to human visual inspection [11]. Texture analysis is a branch in the field of radiomics and it is based on the extraction and processing of the pixels' intensity variations, thus providing a quantitative and detailed description of the image content [12]. In recent years this technique has been integrated into computer-aided diagnosis (CAD) [13]. Through specific algorithms, the CAD-based applications involving medical images aim to offer a more objective description of certain pathological processes and may increase the accuracy of their diagnosis. The basic principle of CT-based texture analysis is that a pathological process that alters the tissue (in this case, the fluid) alters the local image densities, which will in turn give textural features different values from those of the normal structure [14].

In the present research work, texture analysis applied to CT examinations was used to quantify the fluid contained in several histological types of ovarian cysts. The purpose was to determine if these texture characteristics can be further integrated into a CAD system to augment the diagnostic accuracy of ovarian lesions.

Methods

This single-institution, retrospective pilot study has been approved by the institutional review board (ethics committee of the Iuliu Hatieganu University of Medicine and Pharmacy Cluj-Napoca; registration number: 50; date: 11 March 2019), and informed consent was obtained from each patient at the time of their examination. A search of our radiology database was conducted to identify all abdominopelvic CT scans containing images of ovarian lesions from November 2016 to May 2019, by using a keyword search with the following words: "ovary", "ovarian", "cyst(s)", "ovarian + cyst/s", and "adnexal". The original search yielded 307 reports. Each report was analyzed by one radiologist, and studies in which the keyword in the report did not refer to an ovarian lesion were excluded (n =94). The remaining 213 studies were reviewed by the same researcher to confirm the lesions' existence. The other exclusion criteria were: the presence of artifacts within the cystic lesions (n = 12), subjects with an uncertain pathological outcome (n = 36), the lack of gynecological follow-up (n = 32), and lesions containing a small quantity of fluid (a maximum diameter of the fluid content of less than 15 mm) (n=49). Based on these criteria, 84 patients were included in the study (mean age 51.21 years, range 23–84 years).

Firstly, patients were divided into four main groups according to clinical and histopathological diagnosis: benign cysts (n=44), borderline tumors (n=9), primary ovarian tumors (n=22), and ovarian metastases (n=9). Primary ovarian tumors and ovarian metastases were also considered together as the malignant cysts group (n=31). Details about the groups of patients, the types of lesions included in each group, and the number of days that elapsed from the CT examination till the pathological analysis of the lesions are detailed in table I.

The physiological (simple) ovarian cysts group included multiple entities, such as cystic follicles, corpus luteum, follicular cysts, corpus luteum cysts, and serous inclusion cysts [7,9]. All these entities were included in the benign group. Although none had undergone pathological analysis, they were all monitored under a well-established protocol, which certified their benign character. No simple cyst exceeded the size of 50 mm, thus according to the ACR criteria [15], their nature was most likely benign and did not require follow-up by default. However, they were recorded at subsequent examinations for the underlying disease where their involution or disappearance was noted. Cysts were followed through imaging modalities such as ultrasonography (n = 19), CT (n = 5), and magnetic resonance (n = 7) along with the underlying disease (n = 16), or at periodic gynecological follow-ups (n = 15). None of the lesions comprised in the metastases group underwent pathological analysis, their diagnosis being straightforward since the primary tumor was previously documented. All the other lesions underwent pathological examination.

All CT scans were performed on the same unit, Siemens Somatom Sensation, 16 slices (Siemens medical solutions, Forchheim, Germany), using a standard imaging protocol. Before the scan, all patients were given an appropriate amount of water to drink to fill the bladder. The CT scan covered the region from the dome of the liver to the ischial tuberosity attachment. Contrast-enhanced CT (CECT) images were obtained following the injection of 80-140 ml of nonionic iodinated contrast material at a concentration of 350 mg/ml [iohexol (Omnipaque 350; Daiichi-Sankyo Health Care, Tokyo, Japan)] at a rate of 2 ml/sec. The parameters of the CT scan were 120 kV, 200 mAs, and a slice thickness of 3 mm. Arterial and venous phase images were obtained during 25–30 sec and 65–75 sec delay, respectively.

The radiomics approach consisted of five steps: image pre-processing, lesion segmentation, feature

extraction, feature selection, and prediction. After the patients' selection, the examinations were individually reviewed by one radiologist. This researcher was blinded to the clinical outcome of the patients. On the venous phase of each CECT examination, the slice containing the most eloquent characteristics of the cystic fluid was selected. Representative slices were saved in DICOM format (Digital Imaging and Communications in Medicine) and imported into a texture analysis software, MaZda version 5 [16,17]. This software allowed the extraction of texture characteristics from a predetermined region of interest (ROI) within the image. The segmentation consisted of a semi-automatic level-set technique integrated into the MaZda software was used for ROI definition and positioning. The ROI was set within the cystic walls and the software automatically delimitated the liquid content from the walls and any other solid components (Figure 1). To minimize the effect of brightness and contrast variations, a gray-level normalization for each ROI was performed using the limitation of dynamics to $\mu \pm 3\sigma$ (μ = gray-level mean; and σ = gray-level standard deviation) [13].

Pixel information was expressed through specific texture parameters which were derived from the gray-level histogram, co-occurrence matrix, run-length matrix, autoregressive model, Haar wavelet, geometry, and the absolute gradient [16]. The Grey Level Co-Occurrence Matrix (GLCM)-derived texture features were extracted by defining six interpixel distances for each of the four directions between the pixels taken into account (horizontal, vertical, 45°, and 135° direction).

The extraction of the texture features was automatically performed by the software after the ROI definition. The analysis of each ROI provided a large number of texture parameters (over 300). To highlight the most appropriate parameters for the comparison of selected groups, their number was reduced by applying the Fisher selection method. Fisher coefficients (F, the ratio of between-class to within-class variance) select a set of 10 features that have high discriminatory power and are also well-correlated with each other [10]. A cut-off value of F>2 was chosen to differentiate between features with poor and good discriminatory potential.

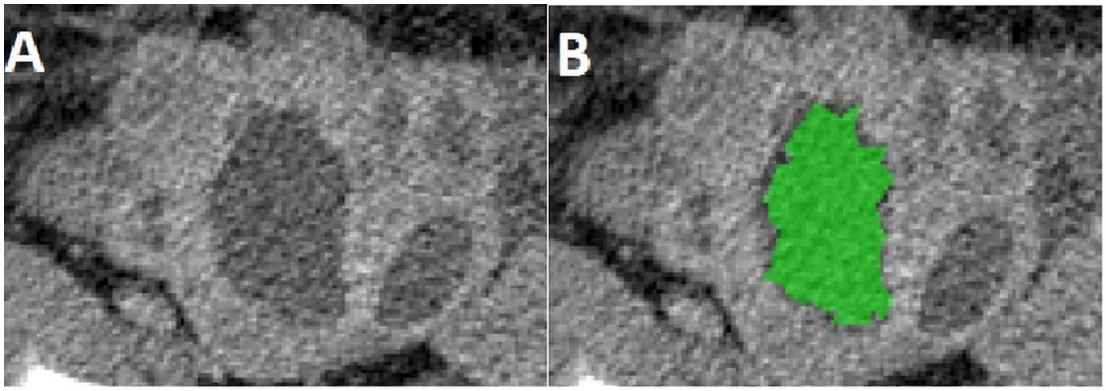

Figure 1. Contrast-enhanced computed tomography image of a 56 years old patient with histologically proven serous carcinoma **(A)**. For texture analysis, one lesion's cystic content is used as the region of interest (green area) **(B)**.

The optimal sets of features obtained from each comparison were further imported into the B11 program (part of MaZda package). The B11 software allows to further process the data by the use of classifiers. A k-nearest-neighbor (k-NN) classifier (which follows the partitioning method for clustering) [10,18] was used to compare vectors of texture features between benign and malignant lesions, primary tumors and metastases, malignant cysts and borderline lesions, and benign cysts and borderline lesions.

The absolute values of the highest-rank parameters were also compared between selected groups by consuming the Mann–Whitney U test. Continuous data were expressed as the median and interquartile range (IQR). The receiver operating characteristic (ROC) analysis was performed, with the calculation of the area under the curve (AUC) with 95% confidence intervals (CIs) for the parameters showing P values below 0.05 on the univariate analysis. The classifier's ability to distinguish between the two histological types of adnexal lesions was shown by quantifying its sensitivity (Se, true positive rate), specificity (Sp, true negative rate), and accuracy (Acc, percentage of correct classified lesions), with 95% CI. Statistical analysis was performed using commercially available dedicated software MedCalc version 14.8.1 (MedCalc Software, Mariakerke, Belgium).

Results

Except for the benign and malignant comparison, all the other compared groups produced only one texture feature that exceeded the F>2 cut-offs. Table I shows the patient groups. Most of the parameters that exceeded the statistical significance threshold were derived from the Co-occurrence matrix (Table II). The k-NN classifier results are displayed in table III. The ROC analysis results are displayed in table IV. The median values for the selected parameters are shown in table V. The ROC curves are displayed in figure 2.

Table I. Main groups of patients, types of lesions contained in each group; diameter (median, range), pathological confirmation measured in days (median, range), and pathological results regarding the cysts' content (in brackets, the percentage of lesions from each disease with the similar findings).

Group	Types of lesions	Number of patients	Diameter (mm)	Pathologic confirmation (days)	Pathological findings
Benign cysts	physiological (simple) cyst	31	31.12 (15-48)	-	-
	serous cystadenoma	3	71.6 (47.5-100.4)	74 (42-113)	serous fluid, 33%; clear fluid, 33%.
	cystadenofibroma	3	62.7 (45.7-84.1)	40 (21-56)	serous fluid, 33%; "green-brown" fluid, 33%.
	mucinous cystadenoma	4	156.35 (130.1-192.2)	58 (14-137)	clear fluid, 25%; rare red blood cells and cellular debris, 25%.
	tubo-ovarian abscess	3	45 (37.9-52.6)	11.22 (9-13)	purulent, 66%.
Borderline tumors	serous borderline tumor	6	63.5 (39.4-110)	23.6 (13-29)	gelatinous content, 75%; mucinous content, 25%
	mucinous borderline tumor	3	41.9 (34.6-45)	26.2 (13-24)	mucinous content, 33%
Primary tumors	serous carcinoma	16	59.42 (25.9-111.8)	80.28 (28-168)	gelatinous content, 13.6%; brownish content, 56.4%; serous fluid, 18%.
	clear cell carcinoma	2	38.9 (31.8-46)	12 (21-3)	clear fluid, 50%; slightly hemorrhagic, 50%
	granulosa cell tumor	2	105.4 (67-143.9)	26.6 (21-32)	serous fluid, 100%;
	mucinous cystadenocarcinoma	2	141 (89-193)	20.5 (9-32)	gelatinous content, 50%; yellow and necrotic content, 50%
Ovarian metastases	colon adenocarcinoma	1	40	42	-
	gastric adenocarcinoma	5	61.81 (33.4-110)	35.4 (16-64)	-
	breast cancer	3	53.75(51-80)	40.33(29-63)	-

Table II. The best-suited features for discriminating between groups and the univariate analysis results. Bold values are statistically significant. DifVarnc, difference variance; Correlat, correlation; InvDfMom, inverse difference moment.

Compared groups	Selected features	Fisher coefficient	p-value
Benign and malignant	S(2,0)DifVarnc	2.12	**<0.01**
	S(2,0)Correlat	2.05	0.77
Primary tumors and metastases	S(0,1)Correlat	2.52	0.08
Malignant and borderline	S(0,3) Correlat	2.15	**0.04**
Benign and borderline	S(2,-2)InvDfMom	3.14	0.28

Table III. Results of the k-NN (k-nearest-neighbor) classification of selected groups using texture features extracted by the Fisher method. All values are expressed as percentages. Between brackets, the values correspond to the 95% confidence interval.

Compared groups	Accuracy	Sensitivity	Specificity
Benign and malignant lesions	64.71 (52.17-75.92)	70.73 (54.46-83.87)	55.56 (35.33-74.52)
Primary tumors and metastases	83.33 (65.28-94.36)	90.48 (69.62- 98.83)	66.67 (29.93-92.5)
Malignant and borderline tumors	73.53 (55.64-87.12)	83.33 (65.28-94.36)	0 (0.01-60.24)
Benign and borderline tumors	80 (56.34-94.27)	87.5 (61.65-98.45)	50 (6.76-93.24)

Table IV. The receiver operating characteristic analysis results. Between the brackets, values correspond to the 95% confidence interval. AUC, area under the curve; S(2,0)DifVarnc, difference variance; S(3;0)Correlat, correlation.

Compared groups	Texture parameter	Significance level	Youden index	Cut-off	Sensitivity	Specificity	AUC
Benign and malignant	S(2,0)DifVarnc	0.0003	0.45	>79.28	59.09% (36.4-79.3%)	86.05% (72.1-94.7%)	0.74 (0.61-0.84)
Malignant and borderline	S(3;0)Correlat	0.0012	0.62	>0.054	75% (19.4- 99.4%)	87.1% (70.2-96.4%)	0.8 (0.63–0.92)

Table V. The median and interquartile range values for the selected parameters.

Compared groups	Individual groups	Individual parameters	Median	Interquartile range
Benign and malignant	Benign cysts	(2,0)DifVarnc	64.17	58.5-68.3
	Malignant cysts		80.34	65.39-84.63
	Benign cysts	S(2,0)Correlat	<0.01	-0.14-0.1
	Malignant cysts		-0.0109	-0.19 – 0.44
Primary tumors and metastasis	Primary tumors	S(0,1)Correlat	-0.11	-0.2 – 0.03
	Ovarian metastases		-0.04	-0.32 – 0.19
Malignant and borderline	Malignant tumors	S(3;0)Correlat	-0.01	-0.16 – 0.18
	Borderline tumors		0.05	-0.00045 – 0.09
Benign and borderline	Benign tumors	S(2,-2)InvDfMom	0.08	0.07 -0.13
	Borderline tumors		0.08	0.05 – 0.1

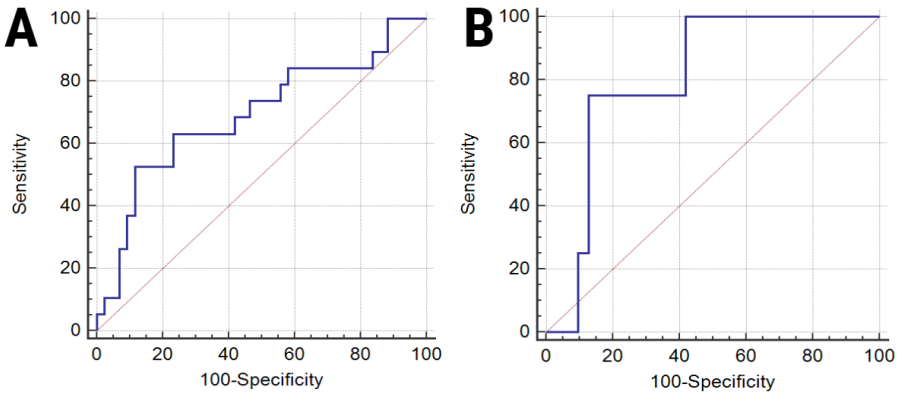

Figure 2. ROC curves displaying the diagnostic value of the (2,0)DifVarnc parameter in differentiating malignant from benign tumors **(A)** and the diagnostic value of the S(3;0)Correlat parameter in differentiating malignant from borderline tumors **(B)**.

When comparing benign and malignant lesions, the k-NN misclassified eight simple cysts, one mucinous cystadenoma, one serous c, all cystadenofibromas, all cases of clear cell carcinoma, one case of mucinous cystadenocarcinoma, six serous carcinomas and one metastasis. The S(2,0)DifVarnc (difference variance) feature held the highest F coefficient (2.12), with median values of 64.17 (IQR, 58.5-68.3) for the benign and 80.34 (IQR, 65.39-84.63) for the malignant group, and showed statistically significant results at the univariate analysis (p=0.00074). The S(2,0)Correlat (correlation) feature had higher values for malignant (median, -0.0055; IQR, -0.14-0.107) than for benign cysts (median, -0.0109; IQR, -0.19 – 0.44), but the comparison of the two groups based on this feature's values was not statistically significant (p=0.7767). For a cut-off of >79.28, the S(2,0)Correlat parameter could identify the malignant lesions with 59.09% sensitivity and 86.05% specificity.

When the texture features extracted from primary tumors and ovarian metastasis were compared, two primary and three secondary lesions were misclassified by k-NN. S(0,1)Correlat was the only parameter that exceeded the F cut-off value, having median values of -0.04 (IQR, -0.32 – 0.19) for metastasis and -0.11 (IQR, -0.2 – 0.03) for primary

tumors, but the comparison of the two entities based on the values of this feature was not statistically significant (P=0.0896).

Comparing malignant and borderline lesions, the k-NN classifier failed to correctly classify all borderline lesions. The only parameter that acceded the cut-off value was represented by S(3;0)Correlat (Correlation, F=2.15), with median values of -0.0192 (IQR, -0.16 – 0.18) for malignant and 0.057 (IQR, -0.00045 – 0.09) for borderline lesions. Based on S(3;0)Correlat's values, de distinction between the two entities was statistically significant (P=0.0488). For a cut-off value of >0.054, the S(3;0)Correlat parameter was able to identify malignant lesions with 75 % sensitivity and 87.1% specificity.

Regarding the distinction between benign and borderline cysts, two lesions from each group were misclassified by k-NN. S(2,-2)InvDfMom (Inverse difference moment) was the dominant feature (F=3.14), having higher values for borderline (median, 0.0852; IQR, 0.07 -0.13) than for benign lesions (median, 0.0816; IQR, 0.05 – 0.1), but the comparison of these values did not hold a statistical significance (P = 0.2858).

Discussion

Our results show that the absolute values of the extracted texture features provide statistically significant results when comparing benign and malignant lesions, and malignant and borderline ones, but failed to provide adequate results when comparing primary tumors and metastases and benign and borderline tumors. Contrarily, the k-NN classifier provided the best results when comparing primary tumors and metastases and benign and borderline tumors. The results shown by conventional statistical analysis and the k-NN classifier may appear contradictory. However, when differentiating between groups, the k-NN classifier considered the entire feature set provided by the Fisher technique, while conventional statistical methods individually analyzed the absolute values of each parameter. The semi-automatic classification system showed a better sensitivity but a lower specificity than common statistical methods. Therefore, we consider that the common statistical methods are best-suited to offer information that are more useful for a future implementation of this protocol.

Computer-aided diagnosis in radiology has made substantial progress in the last decades, from a relatively small research topic to actual implementation in some fields of clinical practice. Currently, numerous software programs are available and offer multiple approaches to CAD [11,19,20], most of them being based on texture classification. The Grey Level Co-Occurrence Matrix (GLCM) is one of the most widespread methods of texture analysis. This method is based on quantifying the distribution and relationships between the gray levels held by the pixels in an image [21]. Difference variance, correlation, contrast, and inverse difference moment are all GLCM-based features [22].

The heterogeneity of an image can be measured by several parameters, one of them being the difference variance, which assigns a higher value for pairs of pixels that deviate more from the average value of the histogram [23]. The higher median values of this parameter obtained by the malignant lesions suggest a more heterogeneous aspect of the fluid (denoting the existence of extreme values of pixel intensities) compared with the relative homogeneity of the benign group. This fact is in accordance with the results of another research involving textural analysis of malignant lesions, the heterogeneity being a well-recognized feature of malignancy [24]. All images of cystadenofibromas were misclassified k-NN. This is also a common issue encountered by classical imaging methods (CT, US, MRI) [5]; even on gross examination at the time of surgery, cystadenofibromas often resemble a malignant lesion [25]. Although the two types of lesions cannot be macroscopically differentiated based on the CT images of their content, the texture maps generated by the MaZda software show visible differences between them (Figure 3).

Another GLCM-based feature, Correlation, was the second dominant when comparing benign and malignant cysts and the dominant feature when malignant and borderline lesions and primary tumors and metastasis were compared. Correlation indicates the linear dependency of grey levels of neighboring pixels and it is often used to measure deformation and displacement [26]. Through this, it reflects the consistency of the textures of an image, with higher values of this feature corresponding to more fine image textures determined by similar gray-level regions [27,28]. The values of this parameter in metastases are higher than in primary tumors, which be caused by the former having a more uniform content, probably because the vast majority of them originated from gastrointestinal tract tumors. A statistically significant result was observed when comparing the absolute values of this parameter between malignant and borderline lesions (P=0.0488). Borderline lesions recorded higher values than malignant lesions, which indicates a higher consistency of their contents. First, this could be motivated by the fact that the vast majority of the borderline lesions included in the study showed a gelatinous content (75%), as opposed to the heterogenous types of fluid found in malignant lesions (mostly serous, but also brownish and yellow). Second, the different types of cellular populations found within the fluid may have influenced the textures, the blood products, necrosis, and malignant cells creating a more turbid appearance of the fluids contained by the lesions from the malignant group. Inverse Difference Moment represents another GLCM-based feature, its values being directly proportional to the level of uniformity of the image [26,29]. Our results showed higher values for borderline than for benign lesions. Again, as in the previous case, this could be a consequence of the fact that all borderline lesions included were of serous type and 75% of them presented gelatinous content on gross examination.

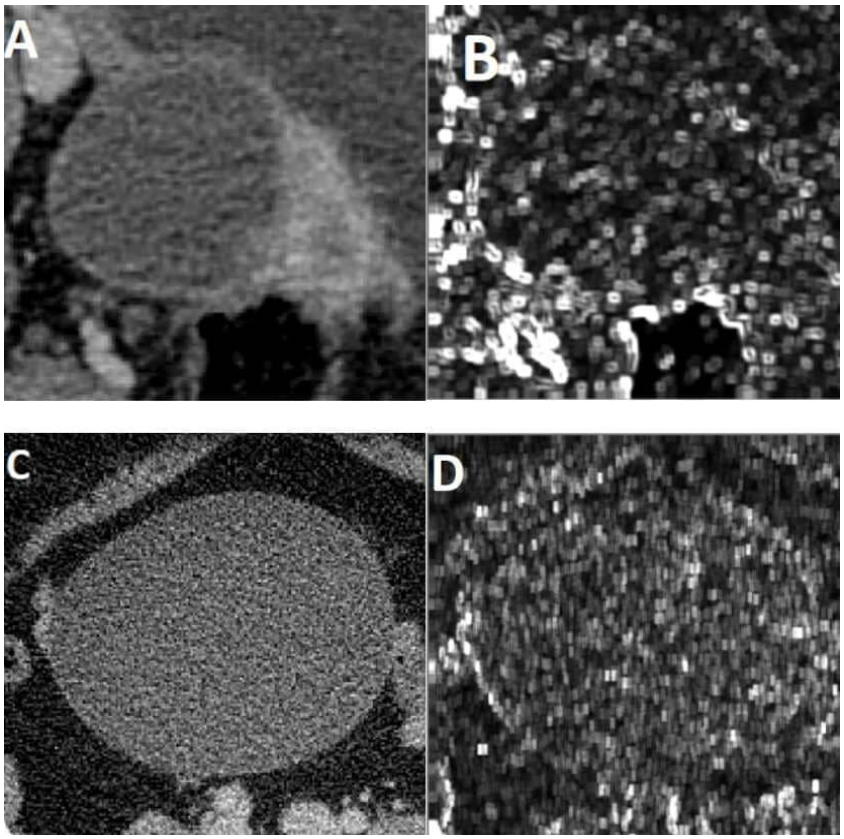

Figure 3. Generated maps showing differences between a malignant and a benign lesion. A) a contrast-enhanced computed tomography image on a 73-year-old patient with pathologically confirmed clear cell carcinoma; and B) generated map based on the S(2,0)DifVarnc (difference variance) feature extracted from this lesion; C) a contrast-enhanced computed tomography image of a 42-year old patient with pathologically confirmed mucinous cystadenoma; and D) generated map based on the S(2,0)DifVarnc feature extracted from this lesion.

Differentiating benign and malignant adnexal masses on CT is a topic of interest for many studies in the literature [4,5,30-32]. The research conducted by Zhang et al. [32] described that Multi-Detector Computed Tomography can accurately classify ovarian lesions into benign and malignant groups with a sensitivity of 86-90% and specificity of 77-84%. Jung et al. [4] reported that contrast-enhanced CT had a sensitivity of 92-95% and a specificity of 74-80% for the diagnosis of malignant adnexal masses. Our results showed lower diagnostic values for the classification of the two entities. These results should be interpreted taking into account that only the liquid content of the cysts was analyzed, and no other morphological features (cystic septations, internal vegetations566 etc.) or ancillary imaging findings (ascites, peritoneal implants, etc.) were considered [4]. In a previous study [33] we were able to demonstrate that the attenuation of the cystic component of ovarian masses on three phases of CECT, benign and malignant lesions could be differentiated with 89.47% sensitivity and 62.5% specificity. However, in the current study, we only used the venous phase of the CECT, thus not being able to assess the contrast dynamics of texture features.

There are very few CAD-based studies in the field that aim to differentiate between benign and malignant ovarian tumors. One research having similar objectives [14] involved processing 3D US images of benign and malign adnexal tumors, which obtained higher accuracy sensitivity and specificity (97%, 94.3%, and 99.7%) compared to our study. This research [14] followed a different approach: features were extracted from a 3D volume that encompassed the entire ovary, the population comprised of both solid and mixed-type tumors, and a different classifier was used (Decision Tree). Also, it included multiple images extracted from the same patient (2000 images from 20 patients). However, a 3D analysis of the lesions may provide additional details that may increase the accuracy of the classification. In a previous study [34] we demonstrated that the texture features of the fluid component of adnexal masses, as extracted from T2-weighted images of magnetic resonance examinations were able to identify malignant lesions with 84.62% sensitivity

and 80% specificity. The better results may be due to the more heterogenous information comprised in MRI images. Following the same workflow but based on ultrasound images, in a previous study [35] we demonstrated that the two groups were discriminated by the same k-NN classifier with 71.43–80% sensitivity and 87.5–89.77% specificity. In both studies [34,35] we obtained more accurate results than the ones observed on CT images. Texture analysis of ovarian cysts remains a hot topic in the radiology research community, with more studies aiming to use this tool in characterizing adnexal masses [36,37].

In our center, the pathological examination mainly includes the analysis of the solid components of ovarian cystic lesions. Consequently, only a part of the included lesions had a description of the gross appearance and cytology of the liquid. Being a retrospective study, it could have had selection bias, especially in the proportion of adnexal malignancies. The fact that no inter or intraobserver agreement was assessed during the lesions' segmentation can also be viewed as a limitation. Manual delineation of the structure of interest contours is not required by this technique, thus not being necessary to assess the inter- or intra-observer reproducibility in the current study. The software used in this study can be regarded as outdated since an official new version has not been released in more than ten years. However, for this research, we used a newly developed beta version released four years ago (MaZda version 5). Although currently several other texture programs have been developed, few others can offer built-in techniques for feature reduction and vector classification within an intuitive interface that can be used by non-image processing specialists, such as medical doctors.

Conclusions

The high discriminative power obtained by the texture parameters indicates that they may be influenced by the histopathological features of a particular group and not only that they reflect the physical properties of the liquids. Also, because possible contamination of the cystic content may result in alterations of the texture parameters, results must be interpreted with caution. However, the preliminary results obtained by the CAD technique indicate that this type of system can distinguish between different types of ovarian cystic lesions based on their content. Moreover, if validated on larger groups of images, the CAD tool can represent an adjuvant component in leading physicians toward a more accurate non-invasive diagnosis.

References

1. Abduljabbar HS, Bukhari YA, Hachim EG, Alshour GS, Amer AA, Shaikhoon MM, et al. Review of 244 cases of ovarian cysts. Saudi Med J. 2015;36:834–838.
2. Valentini AL, Gui B, Miccò M, Mingote MC, De Gaetano AM, Ninivaggi V, et al. Benign and Suspicious Ovarian Masses-MR Imaging Criteria for Characterization: Pictorial Review. J Oncol 2012;2012:481806.
3. Bouic-Pagès E, Perrochia H, Mérigeaud S, Giacalone PY, Taourel P. MR Imaging of primary ovarian tumors with pathologic correlation. J Radiol. 2009;90(7-8 Pt 1):787–802 [French]
4. Jung SI, Park HS, Kim YJ, Jeon HJ. Multidetector computed tomography for the assessment of adnexal mass: is unenhanced CT scan necessary? Korean J Radiol 2014;15:72–79.
5. Togashi K. Ovarian cancer: the clinical role of US, CT, and MRI. Eur Radiol. 2003;13 Suppl 4: L87-L104.
6. Kim KA, Park CM, Lee JH, Kim HK, Cho SM, Kim B, et al. Benign ovarian tumors with solid and cystic components that mimic malignancy. AJR Am J Roentgenol. 2004;182:1259-1265.
7. Russel P. Surface Epithelial—Stromal Tumors of the Ovary. In: Kurman RJ, ed. Blaustein's Pathology of the Female Genital Tract. 4th ed. New York: Springer-Verlag 1994, p. 705-782.
8. Wood D, Fitzpatrick T, Bibbo M Peritoneal Washings and Ovary. In: Wilbur D. Comprehensive Cytopathology E-Book. Elsevier Health Sciences 2014, p. 291-301.
9. Greenebaum E. Aspirating Nonneoplastic Ovarian Cysts: Rationale, Technique, and Controversy. Laboratory Medicine. 1996;27:462–467.
10. Materka A. Texture analysis methodologies for magnetic resonance imaging. Dialogues Clin Neurosci. 2004;6:243–250.
11. Doi K. Computer-aided diagnosis in medical imaging: historical review, current status and future potential. Comput Med Imaging Graph. 2007;31:198–211.
12. Gadkari D. Image Quality Analysis Using Glcm. University of Central Florida Electronic Theses and Dissertations 2004 Jan 1. Available from: https://stars.library.ucf.edu/etd/187.
13. Larroza A, Bodí V, Moratal D. Texture analysis in magnetic resonance imaging: review and considerations for future applications. In: Assessment of Cellular and Organ Function and Dysfunction using Direct and Derived MRI Methodologies, 2016 Oct 26. doi: 10.5772/64641
14. Acharya UR, Sree SV, Saba L, Molinari F, Guerriero S, Suri JS. Ovarian tumor characterization and classification using ultrasound-a new online paradigm. J Digit Imaging. 2013;26:544–553.
15. Harris RD, Javitt MC, Glanc P, Brown DL, Dubinsky T, Harisinghani MG, et al. ACR Appropriateness Criteria® clinically suspected adnexal mass. Ultrasound Q. 2013;29:79–86.
16. Strzelecki M, Szczypinski P, Materka A, Klepaczko A. A software tool for automatic classification and segmentation of 2D/3D medical images. Nuclear Instruments and Methods in Physics Research Section A: Accelerators, Spectrometers, Detectors and Associated Equipment. 2013;702:137–140.
17. Mayerhoefer ME, Breitenseher M, Amann G, Dominkus M. Are signal intensity and homogeneity useful parameters for distinguishing between benign and malignant soft tissue

masses on MR images? Objective evaluation by means of texture analysis. Magn Reson Imaging 2008;26:1316–1322.

18. Karegowda A, Jayaram MA, Manjunath AS. Cascading k-means clustering and k-nearest neighbor classifier for categorization of diabetic patients. International Journal of Engineering and Advanced Technology. 2012;1:147–151.
19. Nioche C, Orlhac F, Boughdad S, Reuzé S, Goya-Outi J, Robert C, et al. LIFEx: A Freeware for Radiomic Feature Calculation in Multimodality Imaging to Accelerate Advances in the Characterization of Tumor Heterogeneity. Cancer Res. 2018;78:4786–4789.
20. Ganeshan B, Skogen K, Pressney I, Coutroubis D, Miles K. Tumour heterogeneity in oesophageal cancer assessed by CT texture analysis: preliminary evidence of an association with tumour metabolism, stage, and survival. Clin Radiol. 2012;67:157–164.
21. Gadelmawla ES. A vision system for surface roughness characterization using the gray level co-occurrence matrix. NDT & E International 2004; 37: 577–588.
22. Alvarenga AV, Pereira WC, Infantosi AF, Azevedo CM. Complexity curve and grey level co-occurrence matrix in the texture evaluation of breast tumor on ultrasound images. Med Phys. 2007;34:379–387.
23. Freeborough PA, Fox NC. MR image texture analysis applied to the diagnosis and tracking of Alzheimer's disease. IEEE Trans Med Imaging. 1998;17:475–479.
24. Skogen K, Schulz A, Dormagen JB, Ganeshan B, Helseth E, Server A. Diagnostic performance of texture analysis on MRI in grading cerebral gliomas. Eur J Radiol. 2016;85:824–829.
25. Wasnik A, Elsayes K. Ovarian cystadenofibroma: A masquerader of malignancy. Indian J Radiol Imaging. 2010;20:297–299.
26. Mohanaiah P, Sathyanarayana P, GuruKumar L. Image texture feature extraction using GLCM Approach. International Journal of Scientific and Research Publications 2013;3:15.
27. Zhao Q, Shi CZ, Luo LP. Role of the texture features of images in the diagnosis of solitary pulmonary nodules in different sizes. Chin J Cancer Res. 2014;26:451–458.
28. Amadasun M, King R. Textural features corresponding to textural properties. IEEE Trans Syst, Man, Cybern 1989;19:1264–1274.
29. Ontobee. Uberon multi-species anatomy ontology Available from: http://www.ontobee.org/ontology/UBERON?iri=http://purl.obolibrary.org/obo/UBERON_0000038
30. Ovarian Serous Cystadenocarcinoma disease: Malacards - Research Articles, Drugs, Genes, Clinical Trials . Available from: https://www.malacards.org/card/ovarian_serous_cystadenocarcinoma
31. Perez-Guillermo M, Orell SR. Male and female genital tract. In: Orell SR, Sterrett GF, editors. Orell and Sterrett's Fine Needle Aspiration Cytology (Fifth Edition) Edinburgh: Churchill Livingstone; 2012, p. 339–369.
32. Zhang J, Mironov S, Hricak H, Ishill NM, Moskowitz CS, Soslow RA, et al. Characterization of adnexal masses using feature analysis at contrast-enhanced helical computed tomography. J Comput Assist Tomogr. 2008;32:533–540.
33. Lupean RA, Ștefan PA, Oancea MD, Măluțan AM, Lebovici A, Pușcaș ME, et al. Computer Tomography in the Diagnosis of Ovarian Cysts: The Role of Fluid Attenuation Values. Healthcare (Basel). 2020;8:398.
34. Lupean RA, Ștefan PA, Feier DS, Csutak C, Ganeshan B, Lebovici A, et al. Radiomic Analysis of MRI Images is Instrumental to the Stratification of Ovarian Cysts. J Pers Med. 2020;10:127.
35. Ștefan PA, Lupean RA, Mihu CM, Lebovici A, Oancea MD, Hîțu L, et al. Ultrasonography in the Diagnosis of Adnexal Lesions: The Role of Texture Analysis. Diagnostics (Basel). 2021;11:812.
36. Seo M, Choi MH, Lee YJ, Jung SE, Rha SE. Evaluating the added benefit of CT texture analysis on conventional CT analysis to differentiate benign ovarian cysts. Diagn Interv Radiol. 2021;27:460-468.
37. Rihana S, Moussallem H, Skaf C, Yaacoub C. Automated algorithm for ovarian cysts detection in ultrasonogram. 2013 2nd International Conference on Advances in Biomedical Engineering, Tripoli, Lebanon, 2013, p. 219-222, doi: 10.1109/ICABME.2013.6648887.